Hindawi Publishing Corporation
Shock and Vibration
Volume 2016, Article ID 6018291, 11 pages
http://dx.doi.org/10.1155/2016/6018291

Research Article

Fracture Propagation Characteristic and Micromechanism of Rock-Like Specimens under Uniaxial and Biaxial Compression

Xue-wei Liu,[1] Quan-sheng Liu,[1,2] Shi-bing Huang,[1] Lai Wei,[1] and Guang-feng Lei[1]

[1] *State Key Laboratory of Geomechanics and Geotechnical Engineering, Institute of Rock and Soil Mechanics, Chinese Academy of Sciences, Wuhan, Hubei 430071, China*
[2] *The Key Laboratory of Safety for Geotechnical and Structural Engineering of Hubei Province, School of Civil Engineering, Wuhan University, Wuhan, Hubei 430072, China*

Correspondence should be addressed to Xue-wei Liu; liuxw87@126.com

Received 14 September 2015; Revised 14 January 2016; Accepted 14 January 2016

Academic Editor: Marcello Vanali

This paper presents a set of uniaxial and biaxial compression tests on the rock-like material specimens with different fracture geometries through a rock mechanics servo-controlled testing system (RMT-150C). On the basis of experimental results, the characteristics of fracture propagation under different fracture geometries and loading conditions are firstly obtained. The newly formed fractures are observed propagating from or near the preexisting crack tips for different specimens, while the propagation paths are affected by the loading condition obviously. Then, by adopting acoustic emission (AE) location technique, AE event localization characteristics in the process of loading are investigated. The locations of AE events are in good agreement with the macroscopic fracture propagation path. Finally, the micromechanism of macroscopic fracture propagation under uniaxial and biaxial compression conditions is analyzed, and the fracture propagation can be concluded as a result of microdamage accumulation inside the material. The results of this paper are helpful for theory and engineering design of the fractured rock mass.

1. Introduction

As the main object for engineering construction, the rock mass contains a large number of structural planes, which form the fracture network. As we know, the interaction of fracture network will reduce strength and stability of rock mass. The rock mass stress around the excavation face will change from triaxial pressure to the biaxial pressure because of the engineering disturbances, which will cause the fracture network propagation. It is clear that the fracture propagation will decrease the strength of rock mass. Therefore, fracture network propagation became the main factor which affects the engineering safety. It is particularly important for engineering safety to study the fracture propagation characteristics and mechanism under complex stress states.

In the last decades, there are a large number of studies on the fracture propagation mechanism. According to the research methods, these studies can be divided into the following two types. The first type is the numerical simulation. For example, Sato et al. [1] discussed the influences of mechanical interaction between fractures to the fracture propagation using the displacement discontinuity comparison method. Van de Steen et al. [2] simulated a confined compression test using two-dimensional boundary element method (BEM) code, and a series of numerical experiments were carried out to determine the influence of crack orientation, the residual friction angle, the dilation angle, and the confining pressure on fracture initiation and propagation mechanism. Wu and Wong [3] modeled fracture initiation, propagation, and coalescence process by the developed numerical manifold method, and the results show that the development of macroshear cracks is preceded by the development of localized deformation bands. Liu et al. [4] investigated the growth of arbitrarily shaped cracks based on the virtual crack closure technique. Haeri et al. [5] studied the mechanism of cracks propagation and coalescence due

to compressive loading of the brittle substances containing preexisting cracks. The results show that crack coalescence stresses and stress intensity factors (SIFs) changed under different loading conditions. Li and Wong [6] modeled the coalescence of two preexisting parallel open flaws in rock subjected to a uniaxial compressive loading and classified the coalescence modes according to their mechanism. Liang et al. [7] and Li et al. [8] discussed the mechanical mechanism of the growth of surface crack using the rock failure process analysis (RFPA) program. Except the above literatures, other researchers using other different numerical methods, like discrete element method (DEM) [9, 10], discontinuous deformation analysis (DDA) [11], finite element method (FEM) [12, 13], and extended finite element method (XFEM) [14], modeled the fracture propagation process and obtained different fracture propagation mechanisms.

Another type of research method is laboratory test. Most of theoretical models are obtained on the basis of experimental results. Yang et al. [15–17] investigated strength and crack coalescence behavior of precracked samples containing single and two coplanar fractures under uniaxial compression, and the photographic monitoring and acoustic emission (AE) technique were adopted for uniaxial compression test. The results are helpful for understanding the failure behavior and fracture mechanism of engineering rock mass. Bobet and Einstein [18, 19] studied the characteristics of fracture coalescence in rock-type materials under uniaxial and biaxial compression and revealed a number of important new physical phenomena. Dyskin et al. propose a series of tests to study two-dimension and three-dimension crack growth mechanism under uniaxial and biaxial compression on different material with simple and multiple preexisting cracks [20–24]. Bombolakis and Brace investigated the brittle crack growth under uniaxial compression [25, 26]. Cao et al. [27] investigated fracture coalescence of rock-like specimens with two and three preexisting flaws under uniaxial compression. Debecker and Vervoort [28] performed a series of uniaxial loading tests to observe the fracture patterns. Wong and Einstein [29] carried out uniaxial compression loading tests on molded gypsum specimens with two coplanar fractures. Wong et al. [30] studied the cracking and coalescence processes of three fractures specimens. Lu et al. [31] studied uniaxial strength and failure in sandstone containing a preexisting 3D surface flaw with help of computed tomography (CT) scanning. Germanovich et al. [32] studied the mechanisms of brittle fracture of rock with preexisting cracks in compression and found that the fracture process in rocks and brittle materials under compression is the competition between a number of mechanisms. Wang et al. [33] investigated the mesodamage mechanism and the cracking characteristics of rock and soil aggregate (RSA) by X-ray CT under uniaxial compressive loading. Ren and Ge [34] studied mesodamage characteristics of sandstone with a single fracture by CT scanning technique.

From the above literatures, we can find the following: (1) The laboratory test is the major way to investigate the fracture propagation mechanism. (2) Most of the tests focus on the fracture propagation mechanism of simple fracture geometries under the uniaxial compression condition. Therefore, fracture propagation mechanism under biaxial compression needs more studies. (3) The main research ways of the tests on the mechanism are scanning the fracture propagation process with CT and scanning the fracture surfaces with SEM. There are a few researches using AE to obtain the fracture propagation laws. Therefore, in this paper, a series of compression tests are carried out on the specimens with single and X-shape cross fractures firstly. Then, the AE event location characteristics are obtained and are used to investigate the micromechanism of fracture propagation.

Table 1: Geometric parameters of fractured specimens.

Fracture type	Inclination angle $\alpha/(^\circ)$	Fracture length L/mm
Single fracture	30, 45, 60, 90	20
Single fracture	45	15, 20, 25, 30
X-shape cross fractures	0, 30, 45, 60	20

2. Experimental Material and Procedure

2.1. Experimental Material. The tested fractured rock mass specimens are with width of 60 mm, height of 120 mm, and thickness of 40 mm and are made in molds using the high-strength gypsum (α-type). As introduced by Liu et al. [35], each sample is cast in a mold with internal dimensions being set to 60 mm × 40 mm × 120 mm, as shown in Figure 1(a). The open flaws are produced with different-sized metallic shims, which are 0.2 mm in thickness, 60 mm in length, and 10–30 mm in width, as shown in Figure 1(b). Then, cure the specimens for a second time and dismantle the molds, and cure specimens under the natural conditions for a month, as shown in Figures 1(c) and 1(d). Besides, the crack tips are planar because of metallic shim, and specimen surfaces are scraped to flat by flat scraper.

To investigate the effect of the preexisting fracture geometry on the fracture propagation process subject to uniaxial and biaxial compression, different geometries including a single fracture and X-shape cross fractures by varying the inclination angle and fracture length were chosen. The preexisting fracture geometries of specimens are shown in Figure 2, and the geometric parameters of fractured specimens are listed in Table 1.

2.2. Testing Equipment and Procedure. The axial compression experiments were carried out on a rock mechanics servo-controlled testing system (RMT-150C) with the maximum vertical loading capacity of 1 MN, as shown in Figure 3(a). This servo-controlled system can test the specimens in load or displacement control while the data are recorded in real-time. In this test, the load control was chosen and all the tests were conducted at a loading rate of 0.02 kN/s. Because the RMT-150C cannot apply the confining pressure, a confining pressure applying system was put at the loading space of the RMT-150C, as shown in Figure 3(b). The confining pressure applying system contains oil pump, pressure stabilizer, oil pipeline, jack, and loading equipment. Three high stiffness plates are strung by four long bolts; as a result, the loading

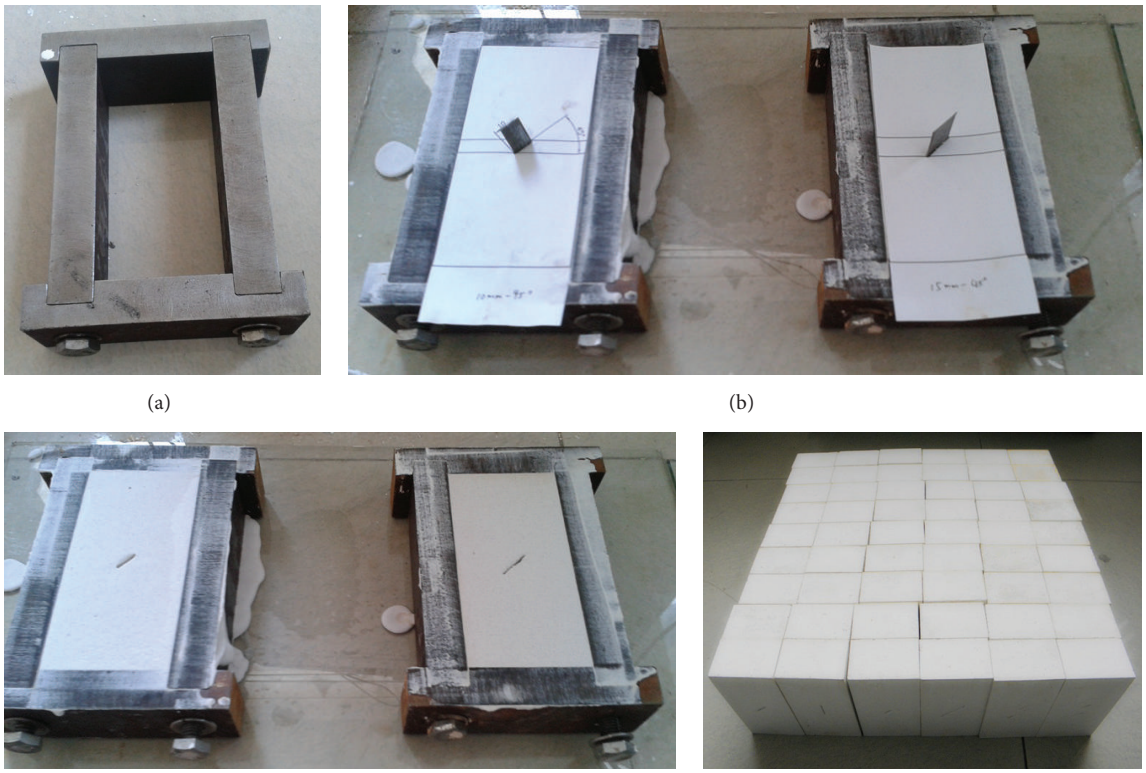

(a) (b) (c) (d)

Figure 1: Preparing process of fracture specimens. (a) Mold of the test. (b) Making flaws. (c) Curing the specimens. (d) Standard specimens.

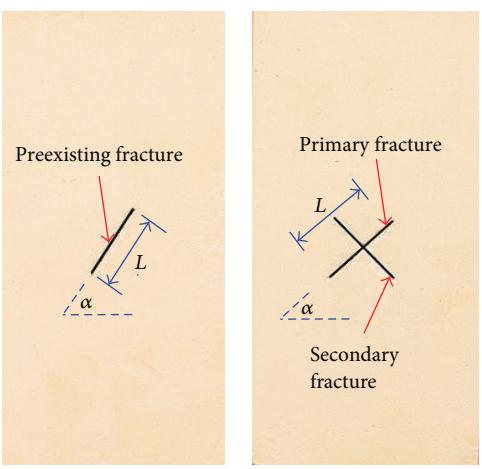

(a) (b)

Figure 2: Specimens with different preexisting fracture geometries. (a) Single fracture specimen. (b) X-shape cross fractures specimen.

equipment has two spaces; one space is for the specimen and another space is for the jack.

Information about fracture initiation, propagation, and geometry during tests is recorded by a multichannel AE monitoring system (namely, PCI-2), as shown in Figure 3(c). The AE system is composed of AE mainframe, AE sensors, preamplifier, and signal acquisition cards, which is able to record the AE hit counts and store AE location automatically. In this study, AE trigger level is set to 40 dB, and the amplitude threshold, the sampling frequency, and the threshold value are set to 18 mV, 2.5 MHz, and 45 dB, respectively.

Four sets of AE sensors are arranged around the specimen, and the layout of the sensors can be seen in Figure 4. As shown in Figure 4, in order to eliminate the influence of the loading on the AE sensors, the distances of sensors 1# and 3# from specimen top surfaces and side surfaces were set to 30 mm and 10 mm, respectively, and sensors 2# and 4# from specimen bottom surfaces and side surfaces were set to 30 mm and 10 mm, respectively. Moreover, two antifriction gaskets were placed between the loading frame and end face of specimen which can decrease the effect of the end friction on the AE monitoring results, as shown in Figure 4(b). At the same time, the Vaseline was used between the sensors and specimen to enhance the monitoring results, as shown in Figure 4(c).

3. Experimental Results

3.1. Characteristics of Fracture Propagation. Figures 5 and 6 show the fracture propagation process of specimens A and B. Specimens A and B are single fracture specimen with inclination angle being 30° and X-shape cross fractures specimen with inclination angle being 45°, respectively.

From Figure 5, it is clear that when $\sigma_1 = 2.45$ MPa, two new fractures initiate from the preexisting crack tips at the

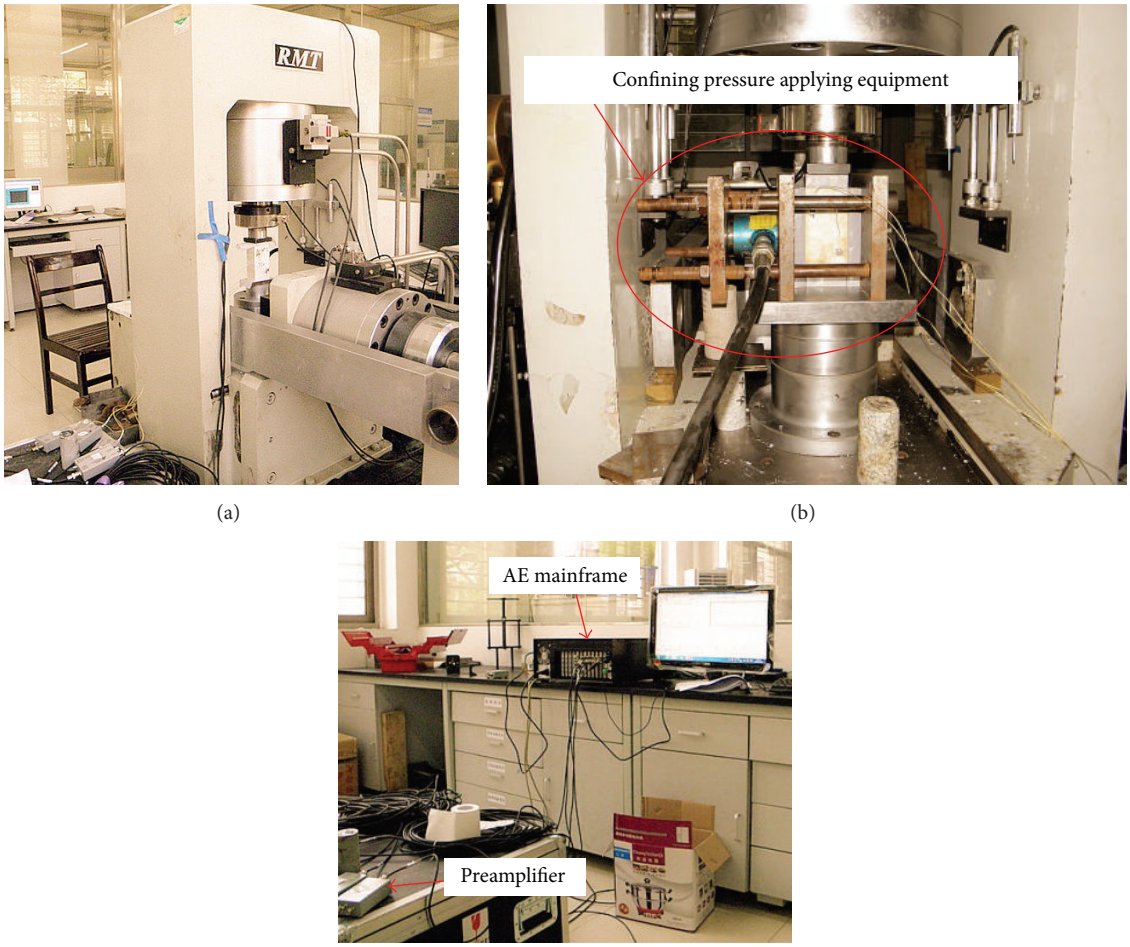

Figure 3: Different testing equipment. (a) RMT-150C rock mechanics servo-controlled testing system. (b) Confining pressure applying system. (c) AE monitoring system.

same time. With the increasing of axial pressure, these two new fractures propagate with the direction of axial loading and no other new fractures initiate in the specimen, as shown in Figures 5(b) and 5(c). In particular, it can be found that several new fractures initiate in the specimen before failure. As shown in Figure 5(d), four new fractures numbered ② and ③ initiate near the preexisting crack tips firstly. Then, two new fractures numbered ④ and ⑤ initiate near fractures ① and ②, respectively. Finally, the continuous loading leads the ultimate failure of specimen and two new fractures numbered ⑥ initiate very fast.

Similarly, it can be found that two new fractures numbered ① initiated from the tips of secondary fracture and a new fracture initiated from the tip of primary fracture, and parts of these new fractures coalesced with each other during propagation, as shown in Figure 6(a). There are no any new fractures initiated while axial pressure reached 3.11 MPa, which is similar to specimen A. When the specimen is loaded to 3.91 MPa, new fracture numbered ③ is initiated, as shown in Figure 6(c). Before the ultimate failure of specimen, 3 new fractures numbered ④ and ⑤ initiate near the preexisting crack tips and then new fracture numbered ⑥ is initiated very fast, as shown in Figure 6(d).

From Figures 5 and 6, the characteristics of fracture propagation during uniaxial compression can be described as follows: (1) The new fractures initiate from or near the preexisting crack tips. The new fractures appeared symmetrically and are relatively small generally, firstly. At the same time, a rumbling sound accompanies the macroscopic fractures propagated, which shows that the fracture propagation process accompanies energy release. (2) The new fractures will coalesce with each other during the process of propagation. Particularly for the X-shape cross fractures specimen, the new fractures which propagate from the primary and secondary fractures will coalesce with each other and become a fracture. With the increase of the axial pressure, the new fractures grow with the direction of axial loading, and the other area will nearly not initiate new fracture. (3) Several new fractures may appear in the specimen before the failure; some of these are initiated near the preexisting crack tips and others are initiated in far area of the specimen. However, these far-field fractures are random and different for different specimens.

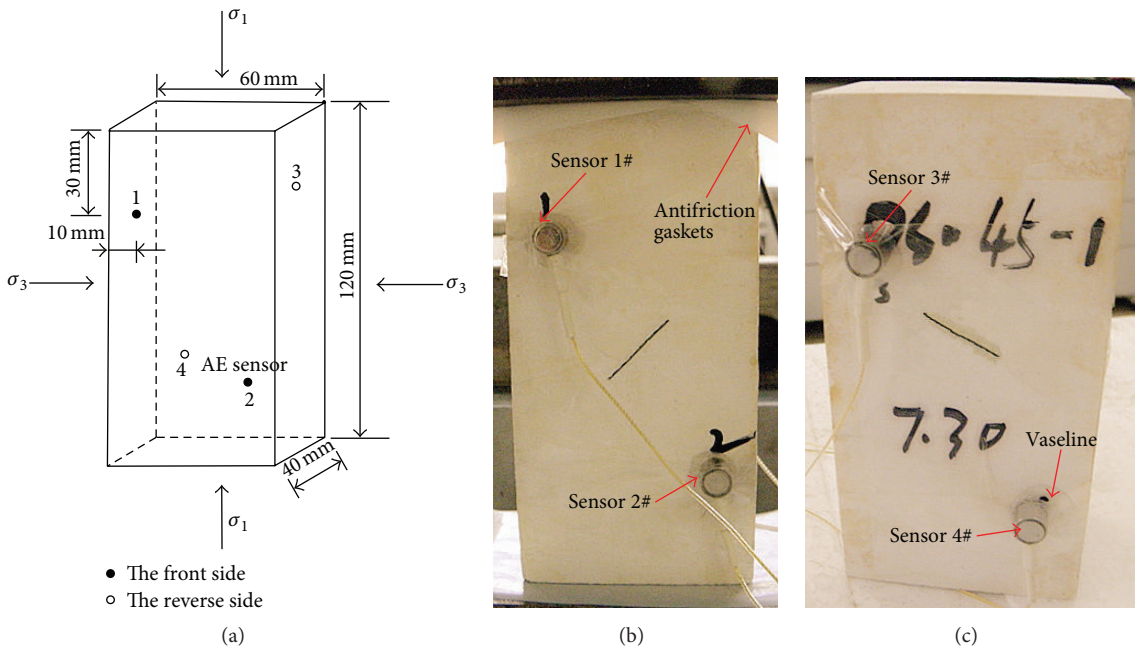

Figure 4: Layout of AE sensors on specimen. (a) The locations of all sensors. (b) Sensors 1# and 2# on the front side. (c) Sensors 3# and 4# on the reverse side.

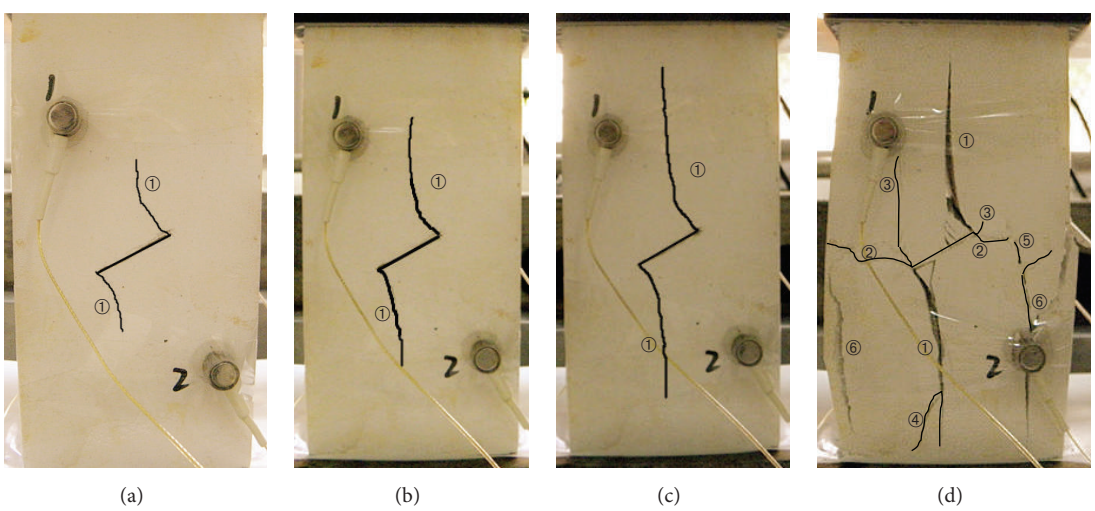

Figure 5: Fracture propagation process of specimen A. (a) σ_1 = 2.45 MPa. (b) σ_1 = 2.87 MPa. (c) σ_1 = 3.33 MPa. (d) Failure.

The final failure modes of specimens C and D are shown in Figure 7. Specimen C is single fracture specimen where inclination angle is 45° and confining pressure is 1 MPa, and specimen D is X-shape cross fractures specimen where inclination angle is 45° and confining pressure is 0.5 MPa.

For specimen C, two new fractures numbered ① initiate from the preexisting crack tips firstly, which is similar to specimen A. Moreover, two areas numbered S1 spall near the crack tips and two fractures ② initiate from this surface spalling S1, respectively. Afterwards, fractures ③ initiate near the center of preexisting crack and fractures ④ initiate far away from the preexisting crack. During the final failure, surface spalling S2, fractures ⑤ and ⑥ are all observed, as shown in Figure 7(a). For specimen D, three new fractures numbered ① are observed to initiate from the preexisting crack tips, which is similar to specimen B. However, the propagation direction of fractures ① is not along the direction of axial loading, which is different from specimen B. Then, two areas numbered S1 spall near the tips of preexisting crack and fracture ①, respectively. Afterwards, fractures ② and ③ initiate from the preexisting crack tip and S1, respectively. Moreover, fractures ② and ③ coalesce with each other at last. The continuous increase of loading leads to ultimate failure of specimen and surface spalling S2 is observed, as shown in Figure 7(b).

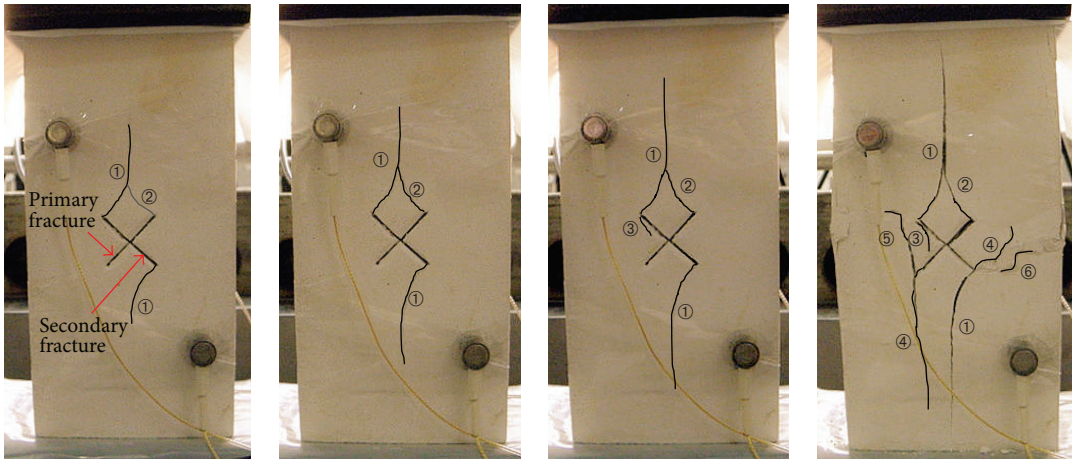

(a) (b) (c) (d)

Figure 6: Fracture propagation process of specimen B. (a) σ_1 = 2.41 MPa. (b) σ_1 = 3.11 MPa. (c) σ_1 = 3.91 MPa. (d) Failure.

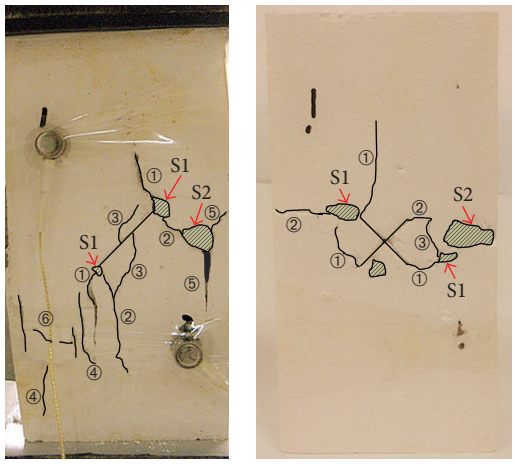

(a) (b)

Figure 7: Failure modes of specimens under biaxial compression. (a) Specimen C. (b) Specimen D.

Compared to specimens A and B, the fracture propagation characteristics show the following differences: (1) The form of new fractures: compared to the uniaxial compression condition, the width and length of new fractures are smaller at the biaxial compression condition. There are no large fractures in the specimen during the loading process and ultimate failure. (2) Fracture propagation path: the coalescence directions of specimens A and B are the direction of the axial loading under the uniaxial compression. However, the fracture propagation directions of specimens C and D are not along the direction of axial loading under the biaxial compression, which means that the confining pressure may control the fracture propagation path in a certain way.

3.2. Characteristic of AE Event Location. The AE events during the loading process are related to the microfracture initiation and propagation in the rock mass. In here, the characteristics of three-dimensional locating of AE events are analyzed with specimen E as an example. In particular, specimen E is single fracture specimen where inclination angle is 45° and fracture length is 20 mm under the uniaxial compression condition. Locations of AE events of specimen E for different loading stages are shown in Figure 8.

The relationship between AE event and loading process of specimen E can be described as follows: (1) At the initial stage, there are a few of AE events and the distribution of AE events is random. (2) The number of AE events increases with the increasing of the axial loading and most of the AE events appear around the preexisting crack tips, which means the microfractures have initiated in the specimen at this stage, as shown in Figure 8(a). (3) When the axial loading increases to the 60% of the peak stress (σ_s), the number of AE events will increase to the 79.3% of the total AE events. There are more

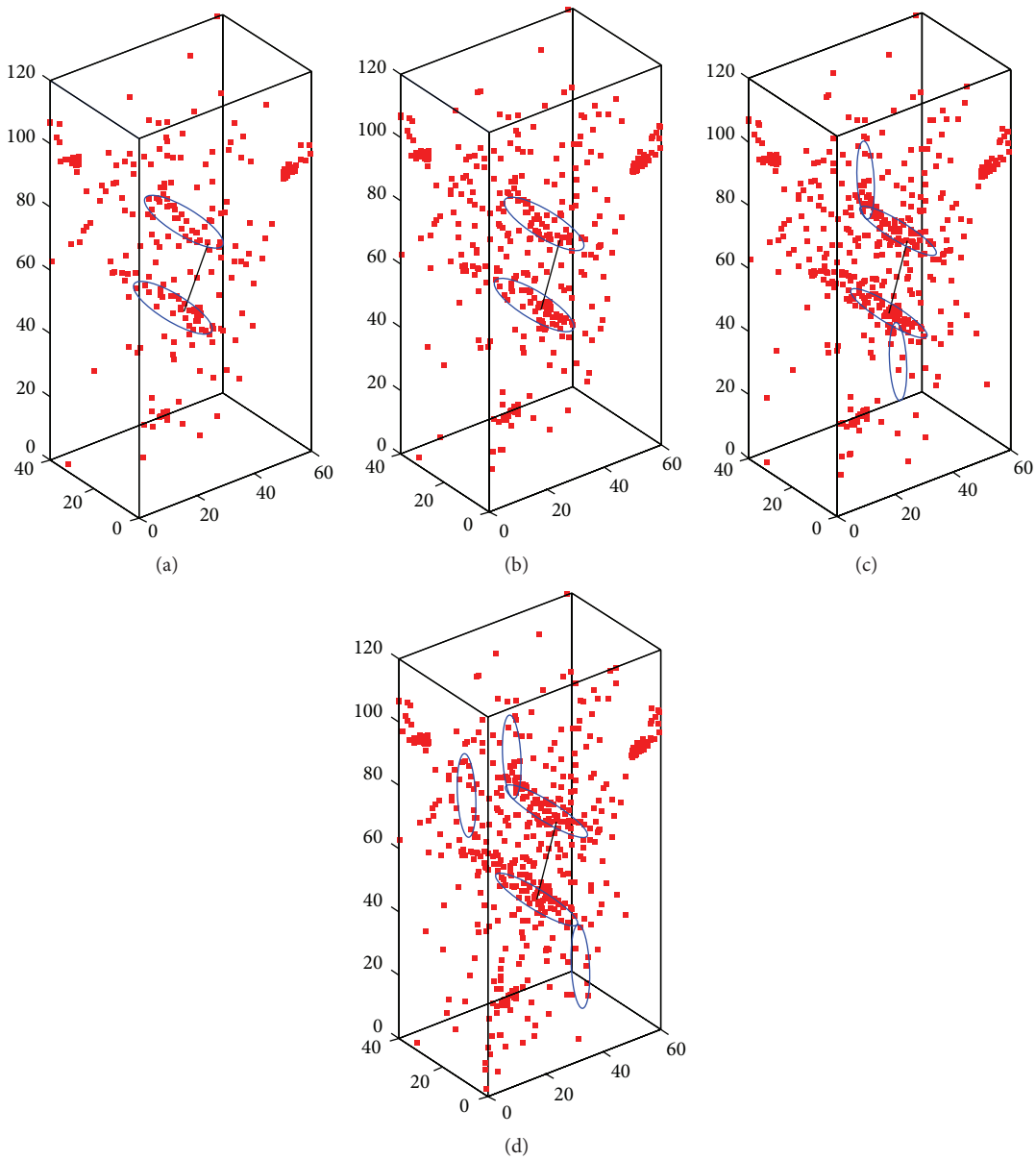

Figure 8: Positions of AE events of specimen E for different loading stages. (a) $\sigma = 30\% \sigma_s$. (b) $\sigma = 60\% \sigma_s$. (c) $\sigma = 80\% \sigma_s$. (d) $\sigma = 100\% \sigma_s$.

AE events around the preexisting crack tips, and AE events are detected in other areas, as shown in Figure 8(b). However, there is no macroscopic fractures initiation in the specimen during this stage. (4) When the axial loading reaches the 80% of the peak stress, the percentage of AE events will increase to the 92.7%, as shown in Figure 8(c). In this stage, there is still no new macroscopic fracture initiation. (5) The macroscopic fractures initiate from the preexisting crack tips when the axial loading reaches the 81.4% of the peak stress. In this stage, the percentage of AE events reaches the 99.6%, and most of them are distributed around the paths of fracture propagation.

Figure 9 shows the macroscopic fracture propagation process of specimen E. Compared with Figures 8 and 9, it can be found that AE location technique is an effective tool to embody the fracture propagation process of fractured specimens. When the axial applied stress reaches 3.12 MPa (corresponding axial stress is 81.4% σ_s), there are two new fractures initiating from the preexisting crack tips, as shown in Figure 9(a). At this time, there are more AE events distributed at the two crack tips and the paths of new fractures indicate the appearance of new fractures, as shown in Figure 8(c). Moreover, some AE events do not seem to correlate with the fracture path, which means the microfractures appear in these regions but the microfractures are not enough for the appearing of macroscopic fractures. Afterwards, it is obvious that the increasing stress leads the AE events to increase rapidly and the AE events locations are in good agreement with the paths of the fracture propagation, as shown in Figures 8(d) and 9(d).

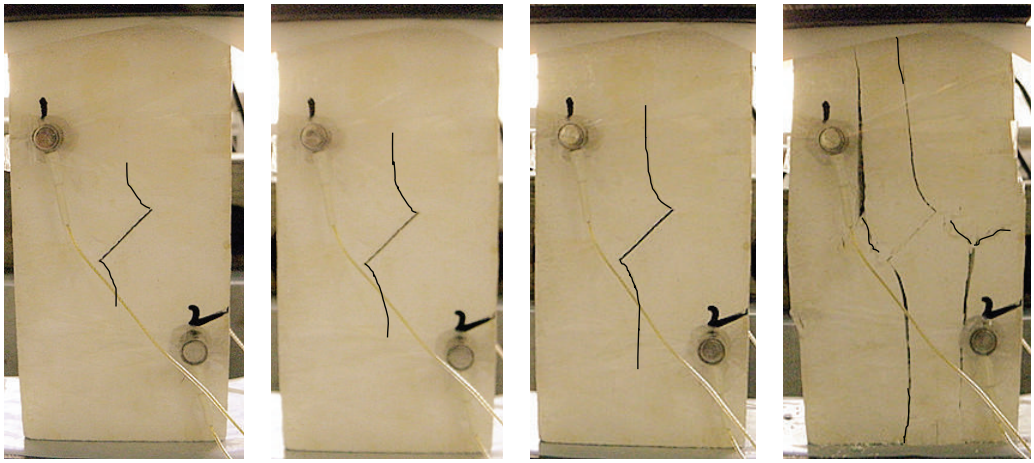

(a) (b) (c) (d)

Figure 9: Fracture propagation process of specimen E. (a) $\sigma = 81.4\% \sigma_s$. (b) $\sigma = 86.3\% \sigma_s$. (c) $\sigma = 92.3\% \sigma_s$. (d) $\sigma = 100\% \sigma_s$.

4. The Microscopic Mechanism of Fracture Propagation

The typical experimental results of specimens B and E are used to analyze the micromechanism of fracture propagation. The AE event ratio k_{AE} is defined as follows:

$$k_{AE} = \frac{n_t}{N} \times 100\%, \quad (1)$$

where n_t is total AE events from the beginning to the time t and N is the total AE events during the whole loading process. At the same time, stress ratio k_σ is defined as follows:

$$k_\sigma = \frac{\sigma_e}{\sigma_s} \times 100\%, \quad (2)$$

where σ_e is the stress at a certain time t and σ_s is the peak stress. The relationships curves between k_σ and k_{AE} are shown in Figure 10.

According to the experimental results, the stress ratios at the time of fracture initiation for specimens B and E are 51.2% and 81.4%, respectively. From Figure 10, it can be found that the corresponding AE ratios with the fracture initiation for both of the specimens are above 80%, which means that there are a large number of AE events appearing in the specimens before the macroscopic fractures propagation. Moreover, the number of AE events from the fracture initiation to the peak stress is obtained, and the AE ratios at this section for the two specimens are less than 10%.

Furthermore, the loading process is divided into 6 stages according to the stress ratio for more analysis. Numbers 1~6 represent the stress ratio stages of 0~10%, 10%~30%, 30%~60%, 60%~80%, and 80%~100% and from the peak stress to the end of loading, respectively. The local AE events ratio is defined as the ratio between AE events during the above 6 stages and the total AE events. According to the experimental results, the 6 local AE event ratios are obtained, as shown in Figure 11. From Figure 11, similar characteristics of local AE

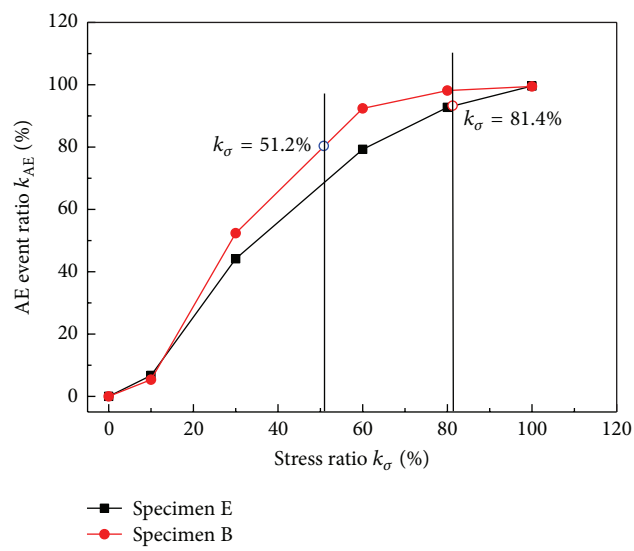

Figure 10: Relationship between stress ratio and AE events ratio.

events ratio for the two specimens can be described as follows. (1) At the first stage, the AE events begin to arise and the local AE event ratios for the two specimens are about 5%. (2) At the second and third stages, the stress ratio is from 10% to 60%, and the AE events begin to increase rapidly. The characteristic for the two specimens at this stage is that the local AE events ratio reaches peak value and the macroscopic fracture initiated in specimen B. (3) After the macroscopic fracture initiation, the local AE event ratio decreased hugely. The local AE event ratios for the two specimens at the sixth stage are 0.41% and 0.53%, respectively.

Generally, the AE events are related to the microfractures initiation and propagation in the specimen. The above experimental results show that most of AE events are detected before the initiation of preexisting crack, which means that the initiation and propagation of macroscopic fractures are

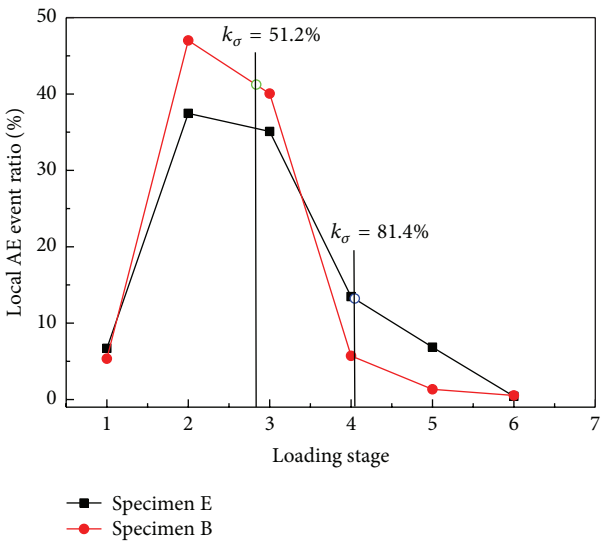

Figure 11: The ratio of AE events of different loading stages.

the result of initiation and propagation of a large number of microfractures. As we know, the microfractures mean the microscopic damage of material. From the above analyses, it can be concluded that the microscopic damage accumulation in the material is the microcosmic condition of the macroscopic fracture initiation.

Therefore, the micromechanism of fracture propagation can be described as follows: (1) The stress in fractured rock mass is changed and redistributed under the disturbance of engineering. (2) The newly formed concentration of stress around the preexisting crack tips caused by disturbance will induce a large amount of microfractures initiation, propagation, and coalescence. (3) The further propagation of microfractures will cause microscopic damage accumulation of material. When the accumulated microscopic damage reaches a certain degree, the macroscopic damage of material (corresponding to the macroscopic fractures) will initiate finally. (4) The energy releasing with the newly macroscopic fracture propagation will cause the stress adjustment, which will cause the further propagation of fractures and failure of rock mass.

5. Discussion

Generally, the fracture propagation mechanism contains tensile and shear failure, which has been approved by most of the researchers. However, the tensile and shear failure mechanisms for fracture propagation cannot describe the changing process inside the specimen before the macroscopic fracture initiation, which means that it is necessary to study the micromechanism of fracture propagation by experiments.

Considering the characteristics of real-time and synchronization for AE location technique, it is feasible to analyze fracture network propagation mechanism under the complex stress conditions. Therefore, AE location technique is used to study the micromechanism in here and AE event characteristics during loading process are obtained. However, the parameters selection and noise filtering during the AE monitoring are empirical and difficult, which affect the precision and limit the application of this method.

According to the experimental results, the micromechanism of fracture propagation is similar for different loading conditions and fracture geometries, but the critical mechanical conditions of fracture initiation have a large difference. Generally, the critical conditions of fracture initiation and paths of fracture propagation are controlled by fracture geometries, stress state, and environment. Therefore, except the present work, the mathematical models for the micromechanism and critical conditions of fracture propagation should be studied in the next work.

6. Conclusions

The present research obtained the characteristics of fracture propagation and micromechanism based on a set of compression tests and AE monitoring tests on the specimens with different fracture geometries. The conclusions are shown as follows.

Under the uniaxial compression, the new fractures are observed from or near the preexisting crack tips with a rumbling sound. With the increase of the axial pressure, the new fractures will propagate with the direction of axial loading and coalesce with each other during propagation. Before the ultimate failure, several new fractures appear in the specimen and some of these are initiated near the preexisting crack tips and others are initiated in far area of the specimen.

Under the biaxial compression, the width and length of new fractures are observed smaller than those of uniaxial compression condition, and the fracture propagation directions are not along the direction of axial loading. There are two fractures observed to initiate near the center of preexisting crack of specimen C, and some surface spalling areas are observed during loading and before the ultimate failure of specimens C and D. Therefore, the confining stresses play a role in the different types of crack propagation.

The AE events location can track the fracture propagation in the specimen in real-time and is in good agreement with the macroscopic fracture propagation process of experiments. At the same time, the experimental results show that the AE ratios are above 80% before the macroscopic fracture initiation, and the AE events decreased hugely after the peak stress, which means that the initiation and propagation of macroscopic fractures are the result of initiation and propagation of a large number of microfractures. Therefore, the micromechanism for the macroscopic fracture propagation can be concluded as a result of microdamage accumulation inside the material.

Conflict of Interests

The authors declare that there is no conflict of interests regarding the publication of this paper.

Acknowledgments

This work was supported by the National Basic Research Program of China (973 Program) Grant no. 2014CB046904, National Nature Science Foundation of China (Grant no. 41130742), and the Key Research Program of the Chinese Academy of Sciences (Grant no. KZZD-EW-05-03). The authors are grateful to the Institute of Rock and Soil Mechanics, Chinese Academy of Sciences (CAS), and Wuhan University, China, as the funding organizations of the project.

References

[1] A. Sato, Y. Hirakawa, and K. Sugawara, "Mixed mode crack propagation of homogenized cracks by the two-dimensional DDM analysis," *Construction and Building Materials*, vol. 15, no. 5-6, pp. 247–261, 2001.

[2] B. Van de Steen, A. Vervoort, and J. A. L. Napier, "Numerical modelling of fracture initiation and propagation in biaxial tests on rock samples," *International Journal of Fracture*, vol. 108, no. 2, pp. 165–191, 2001.

[3] Z. Wu and L. N. Y. Wong, "Elastic-plastic cracking analysis for brittle-ductile rocks using manifold method," *International Journal of Fracture*, vol. 180, no. 1, pp. 71–91, 2013.

[4] Y.-P. Liu, G.-Q. Li, and C.-Y. Chen, "Crack growth simulation for arbitrarily shaped cracks based on the virtual crack closure technique," *International Journal of Fracture*, vol. 185, no. 1-2, pp. 1–15, 2014.

[5] H. Haeri, K. Shahriar, M. F. Marji, and P. Moarefvand, "Cracks coalescence mechanism and cracks propagation paths in rock-like specimens containing pre-existing random cracks under compression," *Journal of Central South University*, vol. 21, no. 6, pp. 2404–2414, 2014.

[6] H.-Q. Li and L. N. Y. Wong, "Numerical study on coalescence of pre-existing flaw pairs in rock-like material," *Rock Mechanics and Rock Engineering*, vol. 47, no. 6, pp. 2087–2105, 2014.

[7] Z. Z. Liang, H. Xing, S. Y. Wang, D. J. Williams, and C. A. Tang, "A three-dimensional numerical investigation of the fracture of rock specimens containing a pre-existing surface flaw," *Computers and Geotechnics*, vol. 45, pp. 19–33, 2012.

[8] G. Li, Z.-Z. Liang, and C.-A. Tang, "Morphologic interpretation of rock failure mechanisms under uniaxial compression based on 3D multiscale high-resolution numerical modeling," *Rock Mechanics and Rock Engineering*, vol. 48, no. 6, pp. 2235–2262, 2015.

[9] L. A. M. Camones, E. do Amaral Vargas, R. P. de Figueiredo, and R. Q. Velloso, "Application of the discrete element method for modeling of rock crack propagation and coalescence in the step-path failure mechanism," *Engineering Geology*, vol. 153, pp. 80–94, 2013.

[10] X.-P. Zhang and L. N. Y. Wong, "Crack initiation, propagation and coalescence in rock-like material containing two flaws: a numerical study based on bonded-particle model approach," *Rock Mechanics and Rock Engineering*, vol. 46, no. 5, pp. 1001–1021, 2013.

[11] X.-L. Zhang, Y.-Y. Jiao, and J. Zhao, "Simulation of failure process of jointed rock," *Journal of Central South University of Technology*, vol. 15, no. 6, pp. 888–894, 2008.

[12] P.-Z. Pan, J. Rutqvist, X.-T. Feng, F. Yan, and Q. Jiang, "A discontinuous cellular automaton method for modeling rock fracture propagation and coalescence under fluid pressurization without remeshing," *Rock Mechanics and Rock Engineering*, vol. 47, no. 6, pp. 2183–2198, 2014.

[13] A. Bobet and H. H. Einstein, "Numerical modeling of fracture coalescence in a model rock material," *International Journal of Fracture*, vol. 92, no. 3, pp. 221–252, 1998.

[14] X. P. Zhou and H. Q. Yang, "Multiscale numerical modeling of propagation and coalescence of multiple cracks in rock masses," *International Journal of Rock Mechanics and Mining Sciences*, vol. 55, pp. 15–27, 2012.

[15] S.-Q. Yang and H.-W. Jing, "Strength failure and crack coalescence behavior of brittle sandstone samples containing a single fissure under uniaxial compression," *International Journal of Fracture*, vol. 168, no. 2, pp. 227–250, 2011.

[16] S.-Q. Yang, "Crack coalescence behavior of brittle sandstone samples containing two coplanar fissures in the process of deformation failure," *Engineering Fracture Mechanics*, vol. 78, no. 17, pp. 3059–3081, 2011.

[17] S. Q. Yang, Y. Z. Jiang, W. Y. Xu, and X. Q. Chen, "Experimental investigation on strength and failure behavior of pre-cracked marble under conventional triaxial compression," *International Journal of Solids and Structures*, vol. 45, no. 17, pp. 4796–4819, 2008.

[18] A. Bobet and H. H. Einstein, "Fracture coalescence in rock-type materials under uniaxial and biaxial compression," *International Journal of Rock Mechanics and Mining Sciences*, vol. 35, no. 7, pp. 863–888, 1998.

[19] A. Bobet, "The initiation of secondary cracks in compression," *Engineering Fracture Mechanics*, vol. 66, no. 2, pp. 187–219, 2000.

[20] E. Sahouryeh, A. V. Dyskin, and L. N. Germanovich, "Crack growth under biaxial compression," *Engineering Fracture Mechanics*, vol. 69, no. 18, pp. 2187–2198, 2002.

[21] A. V. Dyskin, L. N. Germanovich, and K. B. Ustinov, "A 3-D model of wing crack growth and interaction," *Engineering Fracture Mechanics*, vol. 63, no. 1, pp. 81–110, 1999.

[22] A. V. Dyskin, E. Sahouryeh, R. J. Jewell, H. Joer, and K. B. Ustinov, "Influence of shape and locations of initial 3-D cracks on their growth in uniaxial compression," *Engineering Fracture Mechanics*, vol. 70, no. 15, pp. 2115–2136, 2003.

[23] L. N. Germanovich and A. V. Dyskin, "Fracture mechanisms and instability of openings in compression," *International Journal of Rock Mechanics and Mining Sciences*, vol. 37, no. 1-2, pp. 263–284, 2000.

[24] A. V. Dyskin, R. J. Jewell, H. Joer, E. Sahouryeh, and K. B. Ustinov, "Experiments on 3-D crack growth in uniaxial compression," *International Journal of Fracture*, vol. 65, no. 4, pp. R77–R83, 1994.

[25] E. G. Bombolakis, "Study of the brittle fracture process under uniaxial compression," *Tectonophysics*, vol. 18, no. 3-4, pp. 231–248, 1973.

[26] W. F. Brace and E. G. Bombolakis, "A note on brittle crack growth in compression," *Journal of Geophysical Research*, vol. 68, no. 12, pp. 3709–3713, 1963.

[27] P. Cao, T. Liu, C. Pu, and H. Lin, "Crack propagation and coalescence of brittle rock-like specimens with pre-existing cracks in compression," *Engineering Geology*, vol. 187, pp. 113–121, 2015.

[28] B. Debecker and A. Vervoort, "Experimental observation of fracture patterns in layered slate," *International Journal of Fracture*, vol. 159, no. 1, pp. 51–62, 2009.

[29] L. N. Y. Wong and H. H. Einstein, "Crack coalescence in molded gypsum and carrara marble: part 2—microscopic observations

and interpretation," *Rock Mechanics and Rock Engineering*, vol. 42, no. 3, pp. 513–545, 2009.

[30] R. H. C. Wong, K. T. Chau, C. A. Tang, and P. Lin, "Analysis of crack coalescence in rock-like materials containing three flaws—part I: experimental approach," *International Journal of Rock Mechanics and Mining Sciences*, vol. 38, no. 7, pp. 909–924, 2001.

[31] Y. Lu, L. Wang, and D. Elsworth, "Uniaxial strength and failure in sandstone containing a pre-existing 3-D surface flaw," *International Journal of Fracture*, vol. 194, no. 1, pp. 59–79, 2015.

[32] L. N. Germanovich, R. L. Salganik, A. V. Dyskin, and K. K. Lee, "Mechanisms of brittle fracture of rock with pre-existing cracks in compression," *Pure and Applied Geophysics*, vol. 143, no. 1–3, pp. 117–149, 1994.

[33] Y. Wang, X. Li, Y. F. Wu, C. Lin, and B. Zhang, "Experimental study on meso-damage cracking characteristics of RSA by CT test," *Environmental Earth Sciences*, vol. 73, no. 9, pp. 5545–5558, 2015.

[34] J. Ren and X. Ge, "Computerized tomography examination of damage tests on rocks under triaxial compression," *Rock Mechanics and Rock Engineering*, vol. 37, no. 1, pp. 83–93, 2004.

[35] Q. S. Liu, J. Xu, X. W. Liu, J. Jiang, and B. Liu, "The role of flaws on crack growth in rock-like material assessed by AE technique," *International Journal of Fracture*, vol. 193, no. 2, pp. 99–115, 2015.